

Detection of Water Ice in the Lunar Regolith via Microwave Radiometry

Mustafa Aksoy

University at Albany – State University of New York, Albany, NY, 12222, USA

Abstract

Recent lunar observations have concluded that significant water ice deposits may exist in the regolith, especially in the permanently shadowed regions near the lunar poles. Detection and utilization of these reserves is very important to sustain the continuous human presence on the Moon. This paper, using analytical models and numerical simulations, demonstrates that wideband microwave radiometers are promising instruments for exploring underground water ice deposits on the Moon as their brightness temperature spectra are highly sensitive to water presence in the regolith.

1 Introduction

In-situ resource utilization is critical for future lunar missions to establish sustainable human presence on the Moon. Among such resources, water is specifically important considering its potential use for hygiene, fuel production, generating breathable air and drinking water, plant growth, and various other applications [1]. Recent observations of the Moon have implied that substantial water ice deposits may exist in the cold, permanently shadowed regions near the lunar poles [2]. However, these measurements are either limited to the near-surface due to their high frequencies or sensitive to hydrogen rather than water itself [3, 4]; thus, do not provide enough and direct information regarding possible water ice reserves in the regolith, which is believed to be concentrated between the regolith surface and a few meters depth [5]. On the other hand, microwave radiometers can be utilized to detect these deposits owing to larger electromagnetic penetration depths in the regolith at microwave frequencies and the sensitivity of microwave radiations to water ice itself [6]. This paper evaluates this hypothesis through analytical models and numerical simulations. Sections 2 and 3 explain the models used to describe the regolith and the electromagnetic radiation from its surface, and section 4 presents simulations demonstrating the possible use of microwave radiometers to estimate the amount of water ice in the regolith. Finally, section 5 summarizes the conclusions and future implications of the study.

2 Lunar Regolith and Water Ice

The lunar regolith is formed of different fragmented materials and it can be modeled as a layered medium

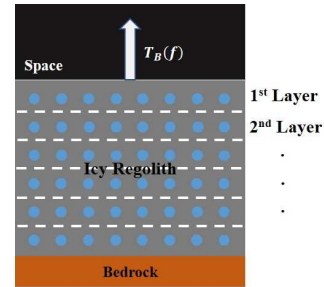


Figure 1. Icy lunar regolith considered in this study. It consists of planar layers described by their density, temperature and water ice content.

where each layer is defined by its physical and thermal properties. In this study, the regolith was assumed to consist of planar layers as shown in Figure 1, and the layers were defined by their density, temperature, and water ice content. Layer thicknesses were accepted as 1 mm to ensure high vertical resolution, and particle sizes were assumed to be at submillimeter scale consistent with previous lunar measurements [7].

Bulk density of the lunar regolith, ρ , was assumed to follow the expression described in [8] versus depth, z :

$$\rho(z) = \rho_d - (\rho_d - \rho_s)e^{-z/H} \quad (1)$$

where ρ_s is the surface density, H is the densification parameter, and ρ_d is the density at depths $z \gg H$. ρ_s and ρ_d were assumed to be 1.30 and 1.92 g/cm³, respectively based on the Apollo measurements [9], and H was accepted as 10 cm in this study. Figure 2 shows the resulting regolith density versus depth.

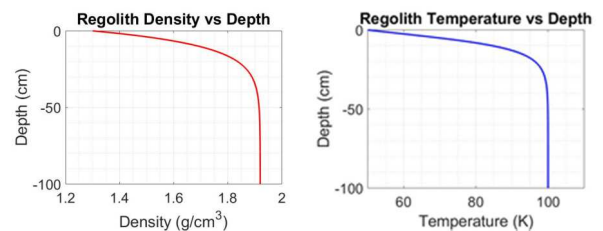


Figure 2. Density and temperature profiles which represent the lunar regolith in a permanently shadowed region near the lunar south pole.

Physical temperature, T , in the lunar regolith versus depth, z , and time, t , can be described by the solution of the following one-dimensional heat conduction equation (neglecting advection):

$$\rho(z)c(z,T)\frac{\partial T}{\partial t} = \frac{\partial}{\partial z}\left(k(z,T)\frac{\partial T}{\partial z}\right) + Q(z,T) \quad (2)$$

where $\rho(z)$, $c(z,T)$, $k(z,T)$, and $Q(z,T)$ are bulk density (g/cm^3), specific heat ($\text{Jg}^{-1}\text{K}^{-1}$), thermal conductivity ($\text{Js}^{-1}\text{K}^{-1}\text{cm}^{-1}$), and internal heat flux ($\text{Js}^{-1}\text{cm}^{-2}$), respectively. A numerical solution process for this equation is given in [10]. A temperature profile representative of a permanently shadowed region near the lunar south pole (latitude 85° S) was generated based on equation (2), as shown in Figure 2, and used in this study.

3 Microwave Radiation Model

Microwave radiometers measure the naturally generated thermal energy emitted from their observation targets and report this energy in terms of brightness temperatures. The brightness temperature, T_B , of a regolith of thickness z_{deep} , observed at normal incidence can be expressed as [11]:

$$T_B = \int_{z_{deep}}^{z=0} \left[\prod_{z'=z}^{z'=0} \Gamma(z') \right] \alpha(z) T(z) e^{-\int_{z'=z}^{z'=0} \alpha(z) dz'} dz \quad (3)$$

where $T(z)$ and $\alpha(z)$ represent the regolith physical temperature and the local microwave attenuation coefficient at depth z , respectively, and $\Gamma(z')$ is the amplitude squared of the Fresnel transmission coefficient coupling the regolith layer at depth z' to its overlying layer. This equation can also be written as:

$$T_B = \int_{z_{deep}}^{z=0} W(z) T(z) dz \quad (4)$$

where $W(z) = \left[\prod_{z'=z}^{z'=0} \Gamma(z') \right] \alpha(z) e^{-\int_{z'=z}^{z'=0} \alpha(z) dz'}$ is the weighting function, and the attenuation coefficient $\alpha(z)$ depends on the relative complex permittivity of the regolith.

In the absence of water ice, the real part of the relative complex permittivity of the regolith, ϵ_r , depends on the bulk density of the regolith, ρ , while its imaginary part in the ilmenite-poor highlands of the lunar polar regions can be expressed as a function of frequency and density [12]. Accordingly, ϵ_r is accepted to be:

$$\epsilon_r = 10^{0.27\rho(z)} (1 - j 10^{0.0043f_{GHz} + 0.312\rho(z) - 2.64}) \quad (5)$$

where f_{GHz} is frequency in GHz. If the water ice present in the regolith is assumed to be in the form of small particles comparable to regolith grains in terms of their size, the complex permittivity of the resulting icy regolith, ϵ_{ir} , can be calculated using Lichtenecker's mixing rule [13]:

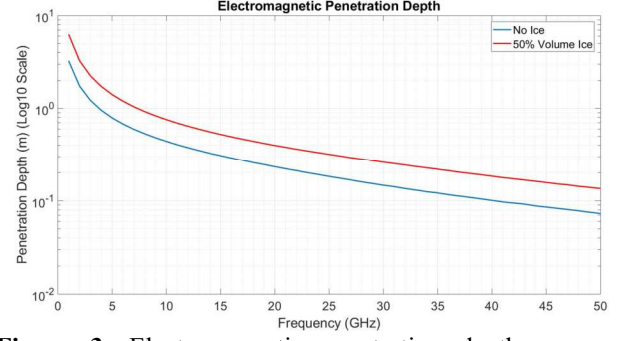


Figure 3. Electromagnetic penetration depths versus frequency for two icy regolith cases with 0% and 50% ice volume fractions. Notice that the penetration depth decreases with frequency and increases with ice volume fraction.

$$\log \epsilon_{ir}(z) = v_r \log \epsilon_r(z) + v_i \log \epsilon_i(z) \quad (6)$$

where ϵ_i is the complex permittivity of the water ice expressed as a function of frequency and temperature in [14], and v_r , v_i are the volume fractions of the regolith and ice, respectively.

Therefore, the weighting function of the icy regolith depends on the density and temperature of the regolith, frequency, and the volume fraction of the ice within the regolith through:

$$\alpha(z) = 2 \times \text{imag} \left\{ 2\pi \frac{f}{c} \sqrt{\epsilon_{ir}(z)} \right\} \quad (7)$$

where f is the radiometer frequency and c is the speed of light in free space. And with the physical temperature profile of the regolith, they determine its surface brightness temperature as expressed in equation (4).

Figure 3 demonstrates the electromagnetic “penetration depth”, i.e., the depth at which the weighting function drops to its maximum value divided by e , for two icy regolith cases with 0% and 50% ice volume fractions in all regolith layers using the density and temperature profiles shown in Figure 1. The penetration depths change from >3 m to ~ 10 cm as frequency increases from 1 GHz

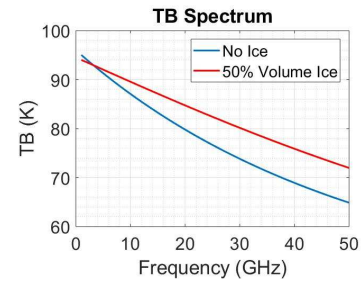


Figure 4. Surface brightness temperature spectrum versus frequency for two icy regolith cases with 0% and 50% ice volume fractions. Notice the change in the slope of the spectrum with increased water ice presence.

to 50 GHz, showing the ability of different frequencies to probe different depths. And the presence of water ice increases the penetration depths as it is found to reduce the electromagnetic attenuation within the regolith.

Figure 4 demonstrates the surface brightness temperatures versus frequency, i.e., the brightness temperature spectrum, calculated for the same two icy regolith cases. Brightness temperatures drop with frequency as higher frequencies, with lower penetration depths associated with them, are sensitive to the colder shallow regolith, whereas lower frequencies, with longer penetration depths, represent the warmer deep regolith. Also, the presence of water ice in the regolith reduces the rate of this drop as larger ice volume fractions lead to lower electromagnetic attenuations and longer penetration depths; thus, increases brightness temperatures at higher frequencies. Such changes in the regolith brightness temperature spectrum based on its water ice content can be utilized using wideband radiometers to quantitatively estimate the amount of water ice the regolith contains.

4 Water Ice Detection and Estimation

Preliminary simulations have been conducted assuming a 1-50 GHz wideband radiometer with 50×1 GHz channels measuring the brightness temperature of the icy regolith with the density and temperature profiles shown in Figure 1. Figure 5 illustrates the change in the slope of the 1-50 GHz brightness temperature spectrum measured by the radiometer as the ice volume fraction within the regolith changes from 0% to 50% in all regolith layers. A least squares retrieval was conducted by modeling radiometer measurements including instrument noise in each frequency channel, and then determining the ice concentration most likely to have produced the simulated noise-corrupted measurement. Figure 6 shows the retrieval results in terms of the probability of obtaining a specific ice volume fraction retrieval accuracy. It can be seen that radiometric uncertainties of 0.15 K or less in all 50 channels result in <1% ice volume fraction retrieval error with >90% confidence. A 0.15 K or better precision

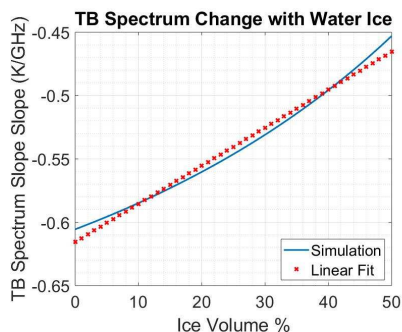


Figure 5. Change in the brightness temperature spectrum with volume water ice fraction in the regolith. In this study the change was assumed to be linear and the linear fit shown in red was used for ice retrieval.

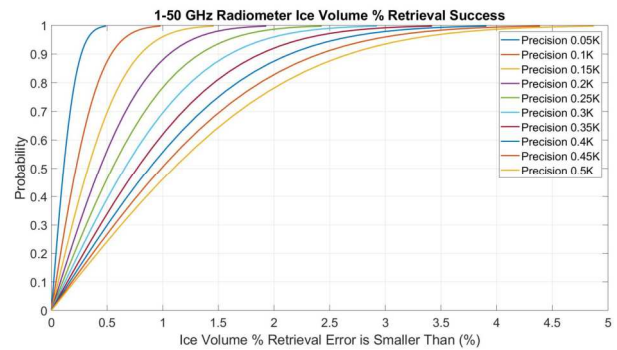


Figure 6. Ice retrieval performance for a 1-50 GHz radiometer with 50 × 1 GHz channels for various radiometer precision scenarios. For instance, 0.15 K or better precision in all radiometer channels result in <1% ice volume fraction retrieval error with >90% confidence. Such precision can be reached with a ~45 msec measurement.

can be reached in a 1 GHz radiometer channel with only ~45 msec measurement assuming a 1000 K system temperature, which would be suitable to investigate large areas on the surface of the Moon in short periods of time.

5 Conclusions and Discussion

This study, using plausible models for the physical and thermal properties of the lunar regolith, has demonstrated that microwave radiometers can be used in future lunar missions to detect and quantitatively evaluate water ice deposits buried in the lunar regolith. It has been shown that brightness temperature spectra measured by wideband radiometers are sensitive to the amount of water ice the regolith contains, and a sample retrieval simulation based on this observation was performed using a 50 GHz bandwidth radiometer. Measurement requirements in this simulation to obtain accurate ice volume fraction estimates were found to be suitable to cover large lunar surface areas within short time periods.

Future lunar radiometers targeting underground water ice deposits on the Moon can be designed and their measurement requirements can be identified by performing similar simulations. However, note that in this study it was assumed that the physical and thermal properties of the regolith such as its density and temperature were known. Moreover, it was accepted that all regolith layers contained the same amount of water ice. Thus, in future lunar missions, auxiliary data from other instruments to characterize such properties may be required for radiometer measurements to be utilized for water ice detection. And, if the depth of a specific ice deposit is known, the frequency band of the instrument can be selected accordingly based on the electromagnetic penetration depths.

6 Acknowledgements

This research has been funded and supported by the National Aeronautics and Space Administration's (NASA) Lunar Data Analysis Program (Grant # 80NSSC20K0312).

7 References

1. S. Belz, B. Ganzer, E. Messerschmid, K. A. Friedrich, U. Schmid-Staiger, "Hybrid life support systems with integrated fuel cells and photobioreactors for a lunar base," *Aerospace Science and Technology*, **24**, 1, Jan 2013, pp. 169-176.
2. S. Li, P. G. Lucey, R. E. Milliken, P. O. Hayne, E. Fisher, J. P. Williams, D. M. Hurley, R. C. Elphic, "Direct evidence of surface exposed water ice in the lunar polar regions," *Proceedings of the National Academy of Sciences*, **115**, 36, Sep 2018, pp. 8907-8912.
3. P. O. Hayne, A. Hendrix, E. Sefton-Nash, M. A. Siegler, P. G. Lucey, K. D. Retherford, J. P. Williams, B. T. Greenhagen, D. A. Paige, "Evidence for exposed water ice in the Moon's south polar regions from Lunar Reconnaissance Orbiter ultraviolet albedo and temperature measurements," *Icarus*, **255**, Jul 2015, pp. 58-69.
4. A. Sanin, I. Mitrofanov, M. Litvak, W. Boynton, J. Bodnarik, D. Hamara, K. Harshman, G. Chin, L. Evans, T. Livengood, T. McClanahan, "How LEND sees the water on the Moon," *In EGU General Assembly Conference Abstracts*, Apr 2016, pp. EPSC2016-7169.
5. K. M. Cannon, D. T. Britt, "A geologic model for lunar ice deposits at mining scales," *Icarus*, **347**, Sep 2020, 113778.
6. X. Gong, D. A. Paige, M. A. Siegler, Y. Q. Jin, "Inversion of dielectric properties of the lunar regolith media with temperature profiles using chang'e microwave radiometer observations," *IEEE Geoscience and Remote Sensing Letters*, **12**, 2, Aug 2014, pp. 384-388.
7. E. A. King Jr, J. C. Butler, M. F. Carman Jr, "The lunar regolith as sampled by Apollo 11 and Apollo 12: Grain size analyses, modal analyses, and origins of particles," *In Lunar and planetary science conference proceedings*, **2**, 1971, p. 737.
8. A. R. Vasavada, J. L. Bandfield, B. T. Greenhagen, P. O. Hayne, M. A. Siegler, J. P. Williams, D. A. Paige, "Lunar equatorial surface temperatures and regolith properties from the Diviner Lunar Radiometer Experiment," *Journal of Geophysical Research: Planets*, **117**, Dec 2012, E12.
9. B. M. French, G. Heiken, D. Vaniman, *Lunar sourcebook: A user's guide to the Moon*, CUP Archive, Apr 1991.
10. P. O. Hayne, J. L. Bandfield, M. A. Siegler, A. R. Vasavada, R. R. Ghent, J. P. Williams, B. T. Greenhagen, O. Aharonson, C. M. Elder, P. G. Lucey, D. A. Paige, "Global regolith thermophysical properties of the Moon from the Diviner Lunar Radiometer Experiment," *Journal of Geophysical Research: Planets*, **122**, 12, Dec 2017, pp. 2371-2400.
11. M. Aksoy, I. Walter, D. M. Hollibaugh Baker, J. R. Piepmeier, "Impact of Water Ice Presence in Lunar Regolith on Surface Brightness Temperatures from 1 to 10 GHz," *LPI Contributions*, **2241**, May 2020, p. 5125.
12. J. Feng, M. A. Siegler, P. O. Hayne, "New constraints on thermal and dielectric properties of lunar regolith from LRO diviner and CE - 2 microwave radiometer," *Journal of Geophysical Research: Planets*, **125**, 1, Jan 2020, e2019JE006130.
13. K. Lichtenecker, "Die dielektrizitätskonstante natürlicher und künstlicher mischkörper," *Physikalische Zeitschrift*, **27**, 1926, pp. 115-158.
14. C. Mätzler, editor, *Thermal microwave radiation: applications for remote sensing*, Iet, 2006.